THE JOURNAL OF PHYSICAL CHEMISTRY B

Article

Cite This: J. Phys. Chem. B 2019, 123, 1527−1536

pubs.acs.org/JPCB

Local and Global Electric Field Asymmetry in Photosynthetic Reaction Centers

Miguel Saggu,[†] Stephen D. Fried,[‡] and Steven G. Boxer*

Department of Chemistry, Stanford University, Stanford, California 94305-5080, United States

Supporting Information

ABSTRACT: The origin of unidirectional electron transfer in photosynthetic reaction centers (RCs) has been widely discussed. Despite the high level of structural similarity between the two branches of pigments that participate in the initial electron transfer steps of photosynthesis, electron transfer only occurs along one branch. One possible explanation for this functional asymmetry is the differences in the electrostatic environment between the active and the inactive branches arising from the charges and dipoles of the organized protein structure. We present an analysis of electric fields in the RC of the purple bacterium *Rhodobacter sphaeroides* using the intrinsic carbonyl groups of the pigments as vibrational reporters whose vibrational frequency shifts can be converted into electric fields based on the vibrational Stark effect and also provide Stark effect data for plant pigments that can be used in future studies. The carbonyl stretches of the isolated pigments show pronounced Stark effects. We use these data, solvatochromism, molecular dynamics simulations, and data in the literature from IR and Raman spectra to evaluate differences in fields at symmetry-related positions, in particular at the 9-keto and 2-acetyl positions of the pigments involved in primary charge separation.

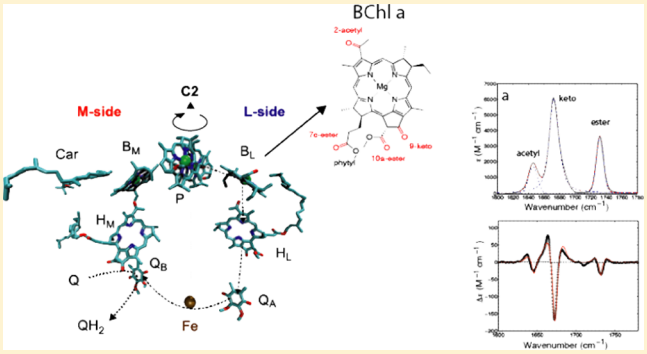

1. INTRODUCTION

The primary charge separation steps of photosynthesis occur in the reaction center (RC),[1] a protein complex that consists of three polypeptides (denoted as H, L, and M subunits), which encases 9 pigments and a nonheme iron in a precise configuration. The photosynthetic pigments comprise four bacteriochlorophylls (P_L, P_M, B_L, and B_M), two bacteriopheophytins (H_L and H_M), two quinones (Q_A and Q_B), and one carotenoid (Figure 1a; an alternative notation replaces L with A and M with B).[2,3] Crystal structures from RCs of the purple bacteria *Rhodobacter sphaeroides* and *Blastochloris viridis* were solved at high resolution in the 1990s[2] and show the presence of an approximate local C_2 symmetry axis between the L and M subunits. Two of the bacteriochlorophylls are arranged in close proximity, forming the special pair (P) that serves as the primary electron donor. The other two bacteriochlorophylls (B_L and B_M) and the bacteriopheophytins (H_L and H_M) are located in two branches on either side of the pseudosymmetry axis (denoted the L-side and M-side or alternatively the A and B side, respectively). A very similar overall chromophore organization is found in both photosystem I (PS I) and photosystem II (PS II) RCs in green plants and cyanobacteria, where chlorophyll *a* replaces bacteriochlorophyll *a* (BChl *a*).

The process of charge separation starts either by energy transfer from the antenna system to the special pair or by direct absorption of light forming the excited state P*.[4] P* decays in 3−4 ps by electron transfer (ET) to $P^+H_L^-$. From H_L^-, the electron moves to Q_A in about 200 ps to form $P^+Q_A^-$.[5] The electron is then passed from Q_A^- to Q_B on a time scale of 100 μs, forming a semiquinone on the Q_B site. B_L plays a significant role in mediating ultrafast ET, though if it is ever reduced; it is, at most, transiently formed.[4,6]

Despite the chemical and structural similarity of the L- and M-branch ET pathways, ET in bacterial RCs occurs predominantly along the L-branch (a ∼65:1 ratio).[4] Understanding the origin(s) of this functional symmetry breaking has been a major challenge for investigators working in the field. Many proposals have been advanced to explain this unidirectional ET, for example, differences in the electronic coupling between cofactors in the L- and M-branches, differences in relative free energies of initial charge-separated intermediates (e.g., $P^+B_L^-$ vs $P^+B_M^-$), asymmetry in the dielectric environments of both branches, or asymmetry in the protein electrostatic or matrix electric fields.[7−9] With respect to the latter point, an early proposal is that the arrangement of protein charges and dipoles creates a potential gradient that favors the charge separation between chromophores on the L side ($P^* \rightarrow P^+H_L^-$) over the M side ($P^* \rightarrow P^+H_M^-$). Calculated electrostatic free energies indicate that ET via H_L is favored by 0.8 eV compared to 0.4 eV via H_M, based on the *B*.

Received: November 27, 2018
Revised: January 13, 2019
Published: January 22, 2019

DOI: 10.1021/acs.jpcb.8b11458
J. Phys. Chem. B 2019, 123, 1527−1536

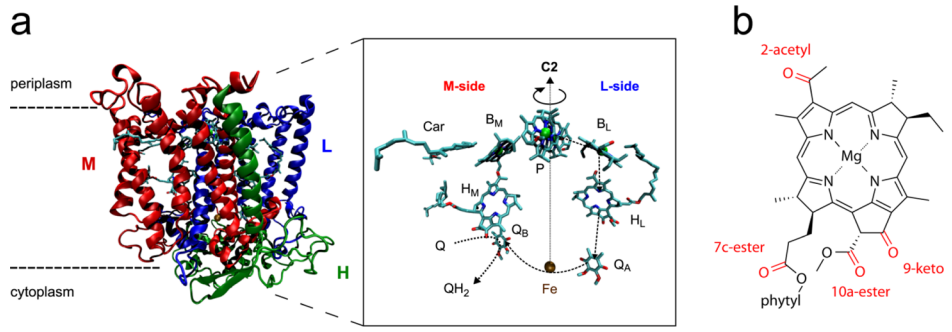

Figure 1. (a) Crystal structure of the photosynthetic RC from *Rb. sphaeroides* with the prosthetic groups arranged in a *C*-2 symmetry (pdb entry 1PCR). (b) Structure of BChl *a* with highlighted carbonyl groups.

viridis crystal structure.[10] However, there has previously been no experimental means to test the calculated differences in electric fields between the L and M sides.

Measurements of electric fields in proteins and model systems based on the vibrational Stark effect have gained attention recently because of the minimal structural perturbation introduced by vibrational reporter groups.[11] Much of the work on proteins has utilized diatomic probes such as nitriles because their vibrational modes occur in a spectral window that is, free of any interfering protein modes, while possessing reasonably large extinction coefficients.[12−14] Nitriles can be introduced on inhibitors (drugs), by site-specific labeling of cysteines as thiocyanates (−SCN), semisynthetically by the introduction of peptides containing noncanonical amino acids or by amber suppression.[13−15] Despite extensive efforts in our lab, it has proved very difficult to place thiocyanate probes in symmetry-related positions near to the functional chromophores in bacterial RCs;[16,17] the recent development of amber suppression in *Rb. sphaeroides* should facilitate the introduction of spectator IR probes.[18]

In this work, we use the intrinsic carbonyl groups of the pigments inside the RC as reporters of electric fields. As seen in Figure 1b, BChl *a*, and bacteriopheophytin *a* (BPhe *a*) each contain 4 carbonyl groups, the 9-keto and 2-acetyl groups, which are part of the conjugated π-system of the macrocycles, an ester at position 10, and the 7c-ester group next to the phytyl side chain. Unlike the electronic transitions of the chromophores, which are coupled to each other,[19,20] the carbonyl groups are relatively isolated and offer ideal probes for estimating the projection of the protein electric field on symmetry-related positions. The vibrational frequencies of the carbonyl groups of the chromophores inside the protein have been assigned in previous work, mainly for *Rb. sphaeroides*, using Fourier transform infrared (FTIR) difference (light-minus-dark) and resonance Raman spectroscopy, and assigned by site-directed mutagenesis that introduced or removed hydrogen bonds to the carbonyls or by wavelength-specific resonance enhancement.[21−23] Following a strategy we have developed elsewhere,[13,24,25] we first measure the sensitivity of each vibration in the isolated chromophores to an external electric field using vibrational Stark spectroscopy giving the Stark tuning rate, $|\Delta\vec{\mu}_{C=O}|$, a measure of the sensitivity of the vibrational transition to an electric field. This is combined with solvatochromism data and molecular dynamics (MD) simulations to produce a calibrated frequency-field conversion. We then use these data to evaluate the difference in field $\vec{F}_L - \vec{F}_M = \Delta\vec{F}_{L-M}$ sensed by each of the intrinsic carbonyl probes at symmetry-related positions on the L and M side of the RC based on observed frequency differences, $\Delta\vec{\nu}^{obs}_{L-M} = \Delta\vec{\mu}_{C=O}\cdot\Delta\vec{F}_{L-M}$, to determine whether there is any evidence for a large difference in the electric field sensed by these probes beyond the local and specific effects of hydrogen bonds. Note that the units we use for the electric field are MV/cm, and for Stark tuning rates, $cm^{-1}/(MV/cm)$. Because both the Stark tuning rate and the field are vector quantities, their relative orientations enter as the dot product for a linear Stark effect. $\Delta\vec{\mu}_{C=O}$ is typically parallel to the carbonyl transition dipole moment that in turn is parallel to the C═O bond axis.[16] The frequency-field calibration also provides an estimate for the absolute value of the fields sensed at different positions, though we will be primarily interested in differences between the L and M sides in the following.

As mentioned above, earlier work from our lab using electronic Stark spectroscopy revealed a difference in dielectric screening of the $P^+Q_A^-$ dipole sensed by a difference in Q_Y electronic spectral shift of the B_L versus B_M and H_L versus H_M, giving effective dielectric constants ε_{eff} around the chromophores, which are in the range of ε_{eff} = 1.5−2.5 for the M-side and ε_{eff} = 4.5−9.5 for the L-side.[8] Effective dielectric constants in this case describe the ratio between calculated electronic band shifts in vacuum and observed band shifts in frozen solution ($\varepsilon_{eff} = \Delta\nu_{calc}(\varepsilon = 1)/\Delta\nu_{obs}$). However, there can be electronic coupling between the chromophores, which influences the electronic spectra and could complicate analysis.[7] In addition, the experimental quantification of electric fields from the UV/vis spectra is limited based on the fact that the exact orientation of the electronic difference dipole is not known with certainty. Vibrational spectroscopy in this work offers the advantage that the difference dipoles of carbonyl groups are always co-linear to the C═O bond and their orientation is known from the crystal structure. Furthermore, the field difference, if any, sensed by these vibrational probes is the intrinsic field difference due to the organized environment around the reactive components in the ground state before any charge separation.

2. MATERIALS AND METHODS

2.1. Extraction and Purification of Photosynthetic Pigments. *Rb. capsulatus* cells were grown semi aerobically as described previously.[26] Cells were harvested and lyophilized after addition of 8 mM trehalose. For extraction of pigments, the lyophilized cells were resuspended in a mixture of methanol/ethyl ether/petroleum ether (5:2:1 v/v).[27] A second extraction with methanol/ethyl ether (5:2 v/v) was performed and both fractions were combined, and 10% NaCl solution was added until phase separation occurred. The ether phase, which

DOI: 10.1021/acs.jpcb.8b11458
J. Phys. Chem. B 2019, 123, 1527−1536

contained the BChl *a* and other hydrophobic pigments, was washed with 10% NaCl solution and dried under vacuum. Pigments were dissolved in 1 mL HPLC solvent (see below) and filtered through a 0.22 μm nylon filter. Purification was carried out using a semi-prep-scale C18 column (Agilent Zorbax 300SB C18, 9.4 × 250 mm, 5 μm) and a multiple wavelength detector (1260 MWD VL). Pigments were detected at 770 nm using isochratic elution with acetonitrile/ethyl acetate/MeOH/water (24:20:47:9 v/v) as the mobile phase at a flow rate of 5 mL/min. The fraction containing BChl *a* was dried under vacuum and stored at −80 °C until further use. BPhe *a* was obtained by the addition of 3% concentrated HCl to BChl *a*. After color change, diethyl ether and water were added, and the ether layer was washed with water until the acid was removed, and the mixture was repurified on HPLC under the same conditions.

Chlorophylls were extracted from fresh spinach by the addition of methanol. The solution was filtered and 1,4-dioxane was added (1:7 v/v).[28] Water was added dropwise until turbidity increased and the solution was placed in a −20 °C freezer for 20 min. During this time, chlorophyll *a* and *b* (Chl *a* and *b*) precipitated out as dioxane complexes and were collected by centrifugation. The precipitate was dissolved in 1 mL HPLC solvent, filtered, and loaded onto HPLC. Separation of chlorophyll *a*/*b* was achieved using the same HPLC setup as described above but with acetonitrile/methanol/ethyl acetate (53:40:7 v/v) as the mobile phase. Pigments were detected at 660 nm using isochratic elution at a flow-rate of 5 mL/min. Pheophytin *a* (Pheo *a*) was obtained by the addition of a few drops of 1 N hydrochloric acid to a solution of Chl *a* in acetone. After color change, diethyl ether and water were added and the ether layer was washed with water until the acid was removed. The sample was repurified on HPLC. The purity of all studied pigments was confirmed by HPLC and UV/vis absorption spectroscopy and was >99%.[27]

Samples of ubiquinone (Q_{10}) and vitamin K_1 were purchased from Sigma-Aldrich at the highest available purity (>98%).

2.2. Vibrational Spectroscopy. All spectra were recorded on a Bruker Vertex 70 FTIR spectrometer equipped with a liquid nitrogen-cooled MCT detector at a spectral resolution of 1 cm^{-1}. For solvatochromism measurements, pigments were dissolved in organic solvents to a concentration of 2−5 mM. For chlorophyll samples, 6 equivalents of pyridine were added in order to maintain a defined coordination shell around the Mg atom and so the pigments were monomeric in a range of bulk solvents. Vibrational spectra were obtained at room temperature by averaging 64 scans and subtracting a reference spectrum consisting of neat solvents without pigments. For vibrational Stark spectroscopy, measurements were carried out at low temperature using a home-built cryostat.[29] A small amount of the sample (~4 μL) was loaded into a home-built cell with two CaF_2 windows (thickness 1 mm, diameter 13 mm, Red Optronics, Mountain View, CA). The windows were coated with a 45 Å Ni layer on the inside to function as a capacitor and separated by two Teflon spacers of 26 μm thickness. Samples were frozen rapidly in liquid nitrogen into organic glasses using 2-methyltetrahydrofuran (2-methyl-THF) or a mixture of dichloromethane/dichloroethane (DCM/DCE, 1:3 v/v). A high-power voltage supply was connected to the cell (Trek Instruments Inc., Medina, NY) and the output voltage was synchronized with the FTIR scanning time. Spectra were acquired in the rapid scan mode and the resulting Stark spectra were the difference between 512 spectra recorded in the presence of an applied field minus 512 spectra recorded under identical conditions without the field.[30] As a control, spectra were recorded at multiple electric field strengths to confirm that the Stark signals scale quadratically with the field strength, as expected for an isotropic, immobilized sample.[30] To obtain the Stark tuning rates $|\Delta\vec{\mu}|\cdot f$, where f is the local field correction factor,[31] the spectra were fitted using the in-house written program SpectFit.[32] Because most spectra had overlapping bands, a fitting procedure has been applied in which the absorption and Stark spectra were fit simultaneously, as described previously.[30]

2.3. Solvatochromism and Electric Field Calculations. To model solvent-induced frequency shifts in terms of electric fields and to develop field-frequency calibration curves, we calculated the solvent reaction fields that several organic solvents (cyclohexane, ether, THF, pyridine, acetonitrile, dimethyl sulfoxide (DMSO), chloroform, and DCM) exert onto the carbonyl groups (keto, acetyl, and esters) of BChl *a*, BPhe *a*, Chl *a*, and Pheo *a* by MD simulations. The parameters for Chl *a* and Pheo *a* were taken from Zhang et al.[33] who used an AMBER03-like method to obtain the charges. Valence parameters were derived from previous work by Ceccarelli et al.[34] The bacteriochlorophyll pigments differ from the chlorophyll pigments in two ways: the vinyl group on ring I is replaced with an acetyl group and ring II lacks a degree of unsaturation between atoms C2 and C3 (Figure 1b). In developing models for BChl *a* and BPhe *a*, we opted to maintain much of the parameterization from Zhang and Friesner's work.[7] Using the existing atom types, all necessary bond and angle valence terms were described. Five improper dihedral terms were missing, and their values were inferred by comparison to the closest analogues present in Zhang and Friesner's parameter set (see full parameters in the Supporting Information). Charges were maintained from Zhang and Friesner except for atoms on the acetyl group, C2 and C3 on ring II, and their hydrogens. The charges for the acetyl group were taken from Ceccarelli.[34] For C2 and C3, the original charge was divided equally among the carbon and the new hydrogen atom bound to it. Generalized AMBER parameters (GAFF) to model the solvent molecules were taken from the virtualchemistry.org database.[35]

We simulated solutions consisting of 1500−3000 solvent molecules (to fill a 65 Å cubic box) and 1 pigment molecule and calculated the electric field the solvent projected onto the bond axes of the various C═O bonds of the pigment using methods similar to those previously described.[36] Solvent boxes were first equilibrated for 100 ps at 150 K and then at 300 K in an *NPT* ensemble. Production dynamics evolved the solvation simulations for 2 further ns, during which the solvent field on the carbonyl groups was calculated every 200 fs. Solvent fields compiled in Table S1 refer to their average values over the production trajectories (the distribution of fields is related to inhomogeneous broadening of the vibrational transitions).[25]

3. RESULTS

3.1. Vibrational Stark Spectroscopy of Bacterial Pigments. The carbonyl stretching modes of BChl *a* and BPhe *a* have been assigned in the literature for the isolated pigments in vitro as well as embedded in RCs (mostly for *Rb. sphaeroides*). The vibrational modes of the carbonyls are well separated and the ester modes usually occur between 1750 and 1720 cm^{-1}, the 9-keto mode between 1710 and 1670 cm^{-1},

DOI: 10.1021/acs.jpcb.8b11458
J. Phys. Chem. B 2019, 123, 1527−1536

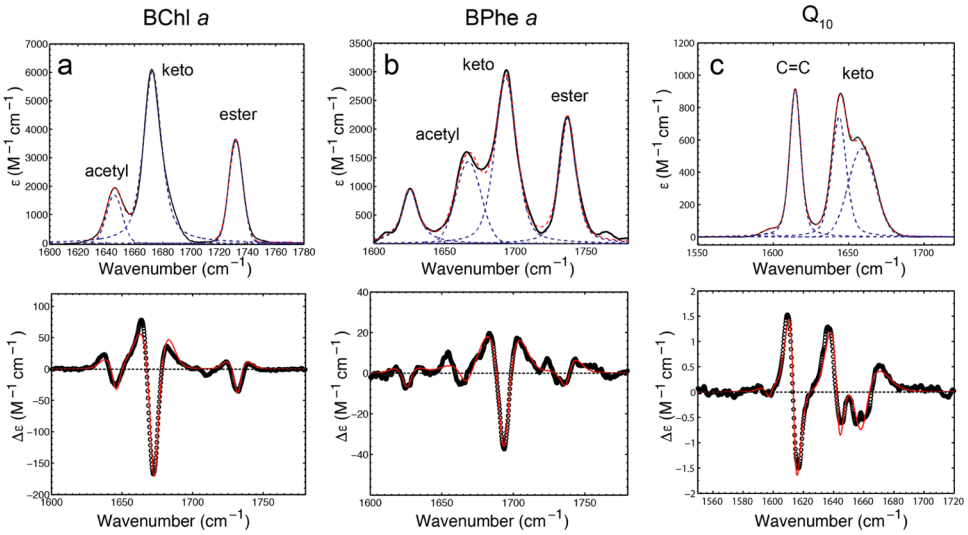

Figure 2. FTIR spectra in the carbonyl region (upper) and vibrational Stark spectra (lower) of photosynthetic chromophores at T = 77 K. (a) 5 mM BChl a in 2-methyl-THF; (b) 4.4 mM BPhe a in 2-methyl-THF; (c) 50 mM Q_{10} in DCM/DCE. Vibrational Stark spectra are overlaid with best fits shown in red giving $|\Delta\vec{\mu}|\cdot f$ (see Table 1). Stark spectra are shown scaled to an external field of 1 MV/cm.

Table 1. Vibrational Frequencies, Extinction Coefficients, and Stark Tuning Rates Extracted from the Fittings of the Experimental Data in Figure 2 (Figure S1 for Green Plant Pigments)

molecule	carbonyl	$\bar{\nu}$ (cm^{-1})	ε (M^{-1} cm^{-1})	$\lvert\Delta\vec{\mu}\rvert\cdot f$ [cm^{-1}/(MV/cm)]
BChl a[a]	9-keto	1672	6100	3.1 ± 0.3
	2-acetyl	1646	1950	2.3 ± 0.2
	ester	1732	3650	1.4 ± 0.2
BPhe$a$[a]	9-keto	1694	3100	2.7 ± 0.3
	2-acetyl	1666	1600	1.8 ± 0.3
	ester	1737	2200	1.2 ± 0.2
ubiquinone Q_{10}[b]	C_1-keto/C_4-keto	1659/1644	550/740	0.99 ± 0.03/0.95 ± 0.03
	C═C	1615	910	0.60 ± 0.03
Chl a[a]	13-keto	1679	3300	2.6 ± 0.2
	ester	1733	2700	1.4 ± 0.2
Pheo a[a]	13-keto	1699	3100	2.1 ± 0.2
	ester	1733	2300	1.0 ± 0.1
vitamin K_1[b]	keto	1659/1653	690/630	0.65 ± 0.03
	C═C	1592	110	0.53 ± 0.03

[a]2Me-THF at T = 77 K. [b]DCM/DCE at T = 77 K

and the 2-acetyl mode between 1650 and 1620 cm^{-1}.[21,27,37] Note that the ester modes are indistinguishable in many solvents, but they can be different when the chromophore is embedded inside the protein because of the anisotropic nature of the environment.[21]

The low-temperature FTIR spectra of BChl a and BPhe a dissolved in 2-methyl-THF are shown in Figure 2a,b. The peaks for the 9-keto, the 2-acetyl and the ester modes are well resolved at 1672, 1646, and 1732 cm^{-1}, respectively (Table 1). The transitions have large extinction coefficients (>2000 M^{-1} cm^{-1}), suggesting large Stark tuning rates, as studies on other vibrational groups have shown a correlation between $|\Delta\vec{\mu}|\cdot f$ and the transition moment (see below).[30,38]

To study the intrinsic sensitivity of the different carbonyl modes to an electric field, we performed vibrational Stark spectroscopy. In general, all vibrational Stark spectra obtained for model systems of carbonyls so far are dominated by the linear Stark effect, that is, the difference polarizabilities $\Delta\bar{\alpha}$ that give rise to quadratic Stark effects are negligible.[39] Consistent with this, the vibrational Stark spectra of BChl a and BPhe a show clearly resolved features, dominated by a second derivative of absorption contribution, which allows robust fitting of the data. Because some of the bands partially overlap, we simultaneously fitted the absorption and Stark spectra with the same data set allowing for a more accurate analysis.[30] The 9-keto group of BChl a exhibits the largest Stark effect with a Stark tuning rate of $|\Delta\vec{\mu}|\cdot f$ = 3.1 cm^{-1}/(MV/cm), the largest tuning rate observed for a carbonyl group to date (Table 1).[24,39] The Stark tuning rates for the 2-acetyl and ester groups are smaller with $|\Delta\vec{\mu}|\cdot f$ = 2.3 cm^{-1}/(MV/cm) and $|\Delta\vec{\mu}|\cdot f$ = 1.4 cm^{-1}/(MV/cm), respectively. Note that the local field correction factor, treated here as a scaler, f, gives the difference between the applied field and the actual field felt by the chromophore being probed. Its value is not certain, but is likely around $f \approx 2$.[25] Because of this uncertainty, Stark tuning rates are reported as $|\Delta\vec{\mu}|\cdot f$. A similar pattern is observed for BPhe a, with all vibrational modes exhibiting slightly smaller Stark tuning rates (Figure 2b). In the Discussion section, we use these experimental values of $|\Delta\vec{\mu}|\cdot f$ as part of a quantitative analysis of the electric fields in the RC of *Rb. sphaeroides*.

DOI: 10.1021/acs.jpcb.8b11458
J. Phys. Chem. B 2019, 123, 1527−1536

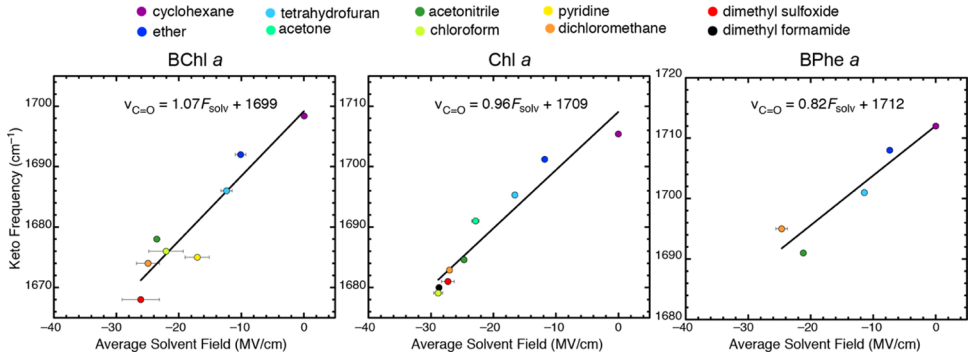

Figure 3. Plots of 9-keto frequencies of pigments dissolved in organic solvents compared against the average electric field the 9-keto group experiences in each of those solvents, calculated by MD simulation.

For completeness, we also studied ubiquinone Q_{10} dissolved in DCM/DCE (Figure 2c). The FTIR spectrum shows two peaks corresponding to the C_1- and the C_4-keto groups at 1659 and 1644 cm^{-1} and another clearly resolved band around 1610 cm^{-1}, which can be attributed to the C═C stretch.[40] The extinction coefficients are much smaller compared to BChl *a* and BPhe *a*, which is reflected in a smaller Stark tuning rate as well (see below). The Stark spectrum shows three resolved features with Stark tuning rates around $|\Delta\vec{\mu}|\cdot f \approx 1.0$ cm^{-1}/(MV/cm) for the keto groups and $|\Delta\vec{\mu}|\cdot f \approx 0.6$ cm^{-1}/(MV/cm) for the C═C stretch. This value is similar to previously reported values for other carbonyl-containing molecules.[24,36] The Stark effect of the C═C stretch is surprisingly large, most likely because this mode is coupled to both keto modes.[5]

3.2. Vibrational Stark Spectroscopy of Plant Pigments. To obtain a complete dataset for the most common pigments in photosynthetic systems and as a comparison to oxygenic photosynthesis, we obtained data for Chl *a* and Pheo *a*. One difference between BChls and Chls is that the latter pigments are missing the 2-acetyl group, which is replaced by a vinyl group. For this reason, the vibrational spectra in the carbonyl region are less complex. Note also that the atom numbering for Chl is different and that the 9-keto group of BChl corresponds to the 13-keto group of Chl. Figure S1 shows the FTIR and vibrational Stark spectra of Chl *a* and Pheo *a* dissolved in 2-methyl-THF and Table 1 lists vibrational frequencies, extinction coefficients, and vibrational Stark tuning rates for the carbonyl groups. As seen for BChl *a*, the largest Stark effect for Chl *a* arises from the 13-keto group and is of comparable magnitude with $|\Delta\vec{\mu}|\cdot f \approx 2.6$ cm^{-1}/(MV/cm). Removing the central Mg atom and transforming Chl *a* into Pheo *a* results in a smaller Stark effect with $|\Delta\vec{\mu}|\cdot f \approx 2.1$ cm^{-1}/(MV/cm), in analogy to BChl *a* versus BPhe *a*.

PS II contains plastoquinone, which has a very similar structure to ubiquinone and is expected to show a comparable Stark effect to ubiquinone. A variety of quinones can be found in photosystems of plants, most of their derivatives of benzoquinone or 1,4-naphthoquinone. Therefore, we performed vibrational Stark experiments on vitamin K_1, which is a derivative of 1,4-naphthoquinone, and can be found in PS I. Vitamin K_1 shows three main bands in the region between 1600 and 1700 cm^{-1}.[40] The bands of the two keto modes can be seen at 1659 and 1653 cm^{-1}; in the lower frequency region, two more bands from the aromatic C═C stretch at 1620 cm^{-1} and the quinone C═C stretch at 1595 cm^{-1} are found. The corresponding vibrational Stark spectra are shown in Figure S1. Vitamin K_1 shows a smaller Stark effect than ubiquinone with the Stark tuning rates $|\Delta\vec{\mu}|\cdot f \approx 0.65$ cm^{-1}/(MV/cm) for the carbonyl stretch and $|\Delta\vec{\mu}|\cdot f \approx 0.53$ cm^{-1}/(MV/cm) for the C═C stretch. As seen for ubiquinone, the C═C stretch shows a comparable Stark effect to the keto groups, most likely because of an admixture of the carbonyl stretch.

3.3. Solvatochromism and Frequency-Field Calibration Curves. Following earlier work, we recorded the IR spectra of Chl *a*, BChl *a*, Pheo *a*, and BPhe *a* in a variety of organic solvents ranging in polarity from cyclohexane to DMSO (the pigments are not soluble in water); the frequencies are compiled in Table S1. Note that for the Mg-containing pigments, several equivalents of pyridine were added to ensure that the pigments were monomeric, avoiding as much as possible aggregates where carbonyl groups from one molecule form complexes with the central Mg atom of another (an interaction that does not occur in RCs; note that the pyridine moieties were not included in the simulations). As has been found for many carbonyl vibrations,[41] we observed consistent red shifts of the carbonyl bands with increased solvent polarity. Using MD simulations to model the solvation environment and calculate solvent reaction fields, we found that solvatochromic trends were well explained in terms of a linear Stark effect.[36] This enabled us to use solvatochromism measurements as reference data to establish field-frequency calibration curves, which extends the vibrational Stark effect method by mapping particular frequencies to absolute electric fields. In the following, we applied this concept to the photosynthetic pigments. The electric fields for the carbonyl groups of all 4 pigments dissolved in 8 different solvents are compiled in Table S2; Figure 3 presents the more significant results.

In general, the 9-keto vibration provided the most robust field-frequency curves with R^2-values clustered around 0.90, and these are displayed in Figure 3. The slope corresponds to the vibration's sensitivity to solvent field, and the intercept to the vibration's frequency in zero electric field. For BChl *a* (Figure 3a), the slope's value [1.1 ± 0.15 cm^{-1}/(MV/cm)] is (2.8 ± 0.6)-fold smaller than the observed Stark tuning rate [3.1 ± 0.3 cm^{-1}/(MV/cm)]. A difference in this range has been observed for all other carbonyl vibrations investigated to date[30] and is believed to reflect—at least partially—the local field effect, that is, present when an external field is used (i.e.,, $f \approx 2$), but not for solvatochromism.[54] The trends in the slopes reflect differences in the keto group's sensitivity on different pigments (e.g.,, the slope is 10−20% less on Chl *a* (Figure 3b) and BPhe *a* (Figure 3c). The lower correlations obtained on photosynthetic pigments relative to previous studies on

DOI: 10.1021/acs.jpcb.8b11458
J. Phys. Chem. B 2019, 123, 1527−1536

acetophenone (R^2 of 0.99)[36] and other carbonyl groups[42] may be due to the inability of MD simulations to describe the more complex solvation structure around a large polyfunctional molecule, or to the possibility that the coordination environment around Mg could be solvent-dependent, implying that the pigments exist as slightly different complexes in different solvents.

The acetyl vibration was not as well resolved in many solvents as it is in the low-temperature spectra in Figure 2, making it impossible to systematically probe its frequency shifts in response to the solvent electric field. The ester vibration, in contrast, is well separated and peak frequencies were more reliably assigned. However, the 7c- and 10a-esters experience significantly different solvent fields in most of our simulations (see Table S2), while their vibrational bands overlap, resulting in a less precise description of their solvatochromism. Nevertheless, R^2 values around 0.6−0.8 were obtained by plotting the ester peak frequencies against the 10a-ester electric field, and the slopes [0.46 $cm^{-1}/(MV/cm)$ for BChl *a*, 0.45 $cm^{-1}/(MV/cm)$ for Chl *a*] were approximately half of those for the 9-keto groups, consistent with the ca. 2-fold lower field sensitivity found in vibrational Stark spectroscopy (Table 1).

4. DISCUSSION

In the present study, we use vibrational Stark spectroscopy to probe electric fields and electric field differences on the L- and M-sides of the RC. Carbonyl vibrational probes are better suited for this purpose than electronic transitions for several reasons. First, the observed vibrational frequencies are not influenced by electronic coupling between the chromophores. Second, the use of localized vibrational reporter groups yields the projection of electric fields at a precise location because the orientation of $\Delta\vec{\mu}_{C=O}$ is known from the X-ray structure as it is parallel to C═O bond axis. In particular, using the intrinsic carbonyl probes of the chromophores, which are part of the ET chain, is ideal because both BChl and BPhe have four independent reporter groups of electric field (9-keto, 2-acetyl and two ester groups). As shown above, the Stark tuning rate of the most relevant 9-keto and 2-acetyl carbonyl groups are found to be large, and the observed frequency shifts report on electric fields, including those due to hydrogen bonds.[36] Because there is a pseudo C_2-symmetry axis between the L- and M-side in the RC, we can directly interpret differences in the vibrational frequencies of the chromophores in symmetry-related positions as differences in the projection of electric fields onto the reporter group. Fourth, as discussed in the following, a large body of data is available in the literature on each vibrational frequency in the RC. The vibrational Stark effect framework brings a different and quantitative perspective to the analysis of absolute shifts and differences on the L- and M-side chromophore environments.

Important symmetry-breaking amino acids (i.e., not conserved between the paralogous chains) in the immediate vicinity of the special pair, the bacteriopheophytins, and H_L and H_M, in particular those near to the carbonyl groups that we are using as probes, are illustrated in Figure 4. While there are significant differences in the vicinities of B_L and B_M, for example, Tyr M210 versus Phe L181, these do not directly interact with the carbonyl groups.[2,43] A large body of literature is available on the measurement and assignment of the vibrational frequencies of the 9-keto and 2-acetyl groups of the BChls and BPhes in the RC from *Rb. sphaeroides*. In particular,

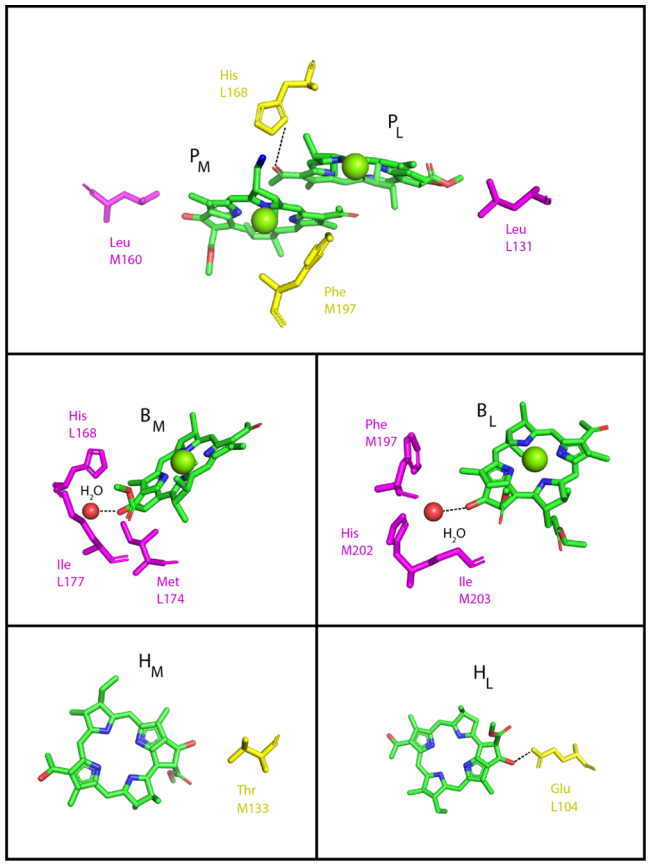

Figure 4. Amino acids that break the symmetry between the L- and M-branches in the vicinity of chromophores in Rb. sphaeroides RCs (pdb entry 2J8C). Symmetry-breaking amino acids are shown in yellow while nonsymmetry-breaking amino acids are shown in magenta. Note that the chromophore alignment is modified from the X-ray structure to better visualize the local environment of the 9-keto groups. For the special pair, the 2-acetyl group of P_L is hydrogen-bonded to His L168 with Phe M197 in the symmetry-related position at P_M. There are no symmetry-breaking amino acids hydrogen bonded to the B_M and B_L residues. For the bacteriopheophytins, protonated Glu L104 hydrogen bonds to the 9-keto group of H_L while the 9-keto group of H_M is not hydrogen bonded.

numerous studies focused on the assignment of hydrogen bonds to the 9-keto and 2-acetyl groups because they are part of the delocalized π-system and any change in H-bonding is expected to affect the redox properties of the chromophores and hence, ET rates.[44] Light-minus-dark FTIR difference spectroscopy, pioneered by Breton et al.[21,45] allows for the assignment of the carbonyl frequencies of the chromophores in the part of the RC, where ET occurs (P_L, B_L, H_L, Q_A, and Q_B).[5,21,45] Vibrational frequencies of the chromophores in the inactive M-branch (P_M, B_M, and H_M) cannot be assigned using this method. In contrast, resonance Raman techniques enable assignment of the carbonyl modes of all chromophores because the ground electronic absorption spectrum shows well-enough resolved bands for all chromophores at low temperature allowing for selective enhancement of vibrational modes of each individual chromophore.[46,47]

Because we are interested in differences in electric fields at symmetry-related positions, we used the data obtained with Raman spectroscopy because we can directly compare differences in vibrational frequencies between the L- and M-side (Table 2). In the following, we will discuss differences in

DOI: 10.1021/acs.jpcb.8b11458
J. Phys. Chem. B 2019, 123, 1527−1536

Table 2. Vibrational Frequencies of the Chromophore Carbonyl Modes in Wild-Type RCs Assigned by Different Groups Using Resonance Raman Spectroscopy (*Rb. sphaeroides* in Black, *Rb. capsulatus* in Red). Differences in the Projection of the Electric Fields onto the Carbonyl Bonds ΔF_{L-M} in MV/cm between Pigments in L- and M-Branches Were Calculated from the Frequency Shifts and the Stark Tuning Rates Summarized in Table 1.

9-keto carbonyl					2-acetyl carbonyl				
P_L	P_M	Δ_{L-M}	ΔF_{L-M} (MV/cm)	Ref.	P_L	P_M	Δ_{L-M}	ΔF_{L-M} (MV/cm)	Ref.
1692	1684	+8	+2.6	46	1636	1660	-24	-10.4	46
1691	1679	+12	+3.9	50-51	1620	1653	-33	-14.3	50-51
1697	1678	+19	+6.1	52	1637	1660	-23	-10.0	53
B_L [a]	B_M [a]	Δ_{L-M} [a]	ΔF_{L-M} (MV/cm)	Ref.	B_L [a]	B_M [a]	Δ_{L-M} [a]	ΔF_{L-M} (MV/cm)	Ref.
1689	1685	±4 [a]	±1.3	46	1660	1663	±3 [a]	±1.3	46
1691	1687	±4 [a]	±1.3	22	1672	1669	±3 [a]	±1.3	52
1693	1689	±4 [a]	±1.3	52	1659	1663	±4 [a]	±1.7	53
1685(7)	1685(7)	±0-2 [c]	±(0-0.6)	54	1662	1662	0	0	54
H_L	H_M	Δ_{L-M}	ΔF_{L-M} (MV/cm)	Ref.	H_L	H_M	Δ_{L-M}	ΔF_{L-M} (MV/cm)	Ref.
1678	1708	-30	-11.1	46	1633	1627	+6	+3.3	46
1678	1703	-25	-9.3	55	1633	1627	+6	+3.3	55
1683	1709 [b]	-26	-9.6	52	1635	1625	+10	+5.6	53
1686	1705	-19	-7.0	56					

[a] L- and M-side not assigned

[b] Shoulder at 1703 cm^{-1}

[c] Both bands lie between 1685-1687 cm^{-1}

electric fields and hydrogen bonding between the pigments on the L- and M-side. Note that one drawback of Raman spectroscopy is the weak Raman intensity of the ester groups. Therefore, our analysis is limited to the 9-keto and 2-acetyl groups of the pigments. We also note that the 2-acetyl and ester carbonyls are on side chains that have conformational flexibility that could result in different projections of the protein field on $\Delta\vec{\mu}_{C=O}$; thus, we primarily focus on the 9-keto carbonyls which are fixed. As noted in Table 2, different investigators have obtained somewhat different values and while most data are available for *Rb. sphaeroides*, we include limited data for closely related *Rb. capsulatus* as well.

In considering what to emphasize, we begin with three important limitations. First, the acetyl groups of the chromophores are rotated out of the plane in several chromophores. This might affect the intrinsic Stark tuning rate and would not be captured by measurements in a frozen glass or solvatochromism in solution. Furthermore, because the measured fields are projections onto $\Delta\vec{\mu}$ differences in orientation of the carbonyl functionality of acetyl groups could affect the analysis. Second, some carbonyl groups are hydrogen bonded and this creates a local electrostatic field that shifts the carbonyl frequency. Within the resolution of the X-ray structures, all of these H-bonds appear to be normal H-bonds and are therefore expected to produce comparable shifts.[36] Third, the fields being reported are local projections sensed by the carbonyl probes. Because primary charge separation involves the creation of large electric dipoles from neutrals, tens of Debye in magnitude, even small field differences can have a substantial effect on the energetics of charge separation. This is in contrast to typical changes in the dipole moment involved in chemical or enzymatic catalysis, where charge shifts over distances on the order of a bond length, at most a change of a Debye, and so larger fields are needed to affect activation free energies.[48,49]

The crystal structure of *Rb. sphaeroides* reveals no hydrogen bonding partners for the 9-keto groups of P_L and P_M (the closest amino acids are leucine L131 and leucine M160 in the symmetry-related position). The modest differences in vibrational frequencies can therefore be attributed to differences in the electrostatic environment, between 8 and 19 cm^{-1} implying $\Delta\vec{F}_{L-M} \approx (2.5-5.9)f$ MV/cm, a relatively minor difference. The 2-acetyl groups show a larger difference in frequency, between 23 and 33 cm^{-1} due, at least in part, to a difference in hydrogen bonding because the 2-acetyl group of P_L is hydrogen bonded to His L168, while the symmetry-related Phe M197 does not form a hydrogen bond to P_M. A comprehensive study by Mattioli et al. investigated the changes in midpoint potentials of P associated with hydrogen bond changes at the carbonyls; the symmetry mutant in which His L168 was replaced by Phe shows that the 2-acetyl frequencies of P_L and P_M are identical, indicating a similar electrostatic environment (both at 1653 cm^{-1}).[50,57] These results suggest that the global electrostatic asymmetry around P is small. The hydrogen bond between the 2-acetyl group of P_L and His L168 may contribute to the stabilization of the charge displacement

DOI: 10.1021/acs.jpcb.8b11458
J. Phys. Chem. B 2019, 123, 1527−1536

associated with excitation of P to P* as observed in electronic Stark spectra of P.[58]

None of the carbonyl groups of the accessory BChls B_L and B_M are hydrogen-bonded. The observed differences in vibrational frequencies are all <4 cm^{-1}, indicating a very similar electrostatic environment for both B_L and B_M in the ground state; the difference in the projection of electric field is $(1-2)f$ MV/cm at both the 9-keto and 2-acetyl group. For *Rb. capsulatus* RCs, the vibrational frequencies of the 9-keto groups differ by less than 2 cm^{-1} and the frequencies of the 2-acetyl groups are identical.[22] This indicates that electrostatic differences projected onto the keto groups of the accessory BChls in the electronic ground state are not of crucial importance for unidirectional ET. The absence of hydrogen bonds is reflected in vibrational frequencies between 1685 and 1690 cm^{-1} for the 9-keto group and 1660 cm^{-1} for the 2-acetyl group. By reference to Figure 3 and Table S1, these frequencies correspond to small electrostatic fields on an absolute basis and are consistent with a relatively nonpolar environment, comparable to that found in ether, for the carbonyl groups.

The 9-keto group of H_L is hydrogen-bonded to the protonated glutamic acid L104, while the symmetry-related threonine M133 is not hydrogen-bonded to H_M. H_L's 9-keto group is concomitantly shifted 20−30 cm^{-1} to the red, suggesting a significant electrostatic field arising from this local hydrogen bonding interaction and a typical hydrogen bond shift. In *Rb. capsulatus,* the symmetry mutant where Glu L104 has been replaced with leucine still shows a difference of ∼14 cm^{-1} between the 9-keto groups, which would correspond to a difference in electric fields of ∼5*f* MV/cm, suggesting that the difference in the electric field projected on the 9-keto carbonyl observed in *Rb. sphaeroides* reflects a combination of local hydrogen bonding and more distal interactions.[56] There are no hydrogen bonding partners for the 2-acetyl group of both H_L and H_M, and the difference in frequency is smaller, 6−10 cm^{-1} ($\Delta\vec{F}_{L-M} \approx (3-5)f$ MV/cm), reflecting small electrostatic differences arising from the protein matrix.

The field-frequency curves reveal that the electric field experienced by B's 9-keto group in the *Rb. sphaeroides* RC is small on an absolute basis on both the L-branch (−7 MV/cm) and M-branch (−11 MV/cm)—comparable to the solvent ether, whereas H_M's 9-keto experiences a similarly small overall electric field (−6 MV/cm), the hydrogen-bonded H_L's electric field is large (−40 MV/cm), though assigning it an absolute value requires extrapolation beyond the domain delineated by the solvent series.

5. CONCLUSIONS

We have quantified differences in electric fields in symmetry-related positions between the active L- and the inactive M-side in the RC of the purple bacterium *Rb. sphaeroides* using the vibrational Stark effect. We used the intrinsic carbonyl groups of the pigments as the reporter of electric fields. The vibrational Stark effects of the carbonyls are large, most likely because of a large electronic contribution of the π-macrocycle to the Stark tuning rate. The overall differences in vibrational frequencies between the L- and M-side are very small for B_L versus B_M. Given the critical role of B_L in mediating primary charge separation, the negligible difference in the field projected on the 9-keto carbonyl group of B_L versus B_M suggests that this is not a primary determinant of bias toward the L-side. An important caveat that is intrinsic to our approach is that we measure the specific projection of the protein electric field onto the C═O bond. Because we do not know *a priori* what the direction of the global field is, it could be that the 9-keto carbonyls of the monomeric bacteriochlorophylls are nearly orthogonal to the field. Thus, the strategy of using these intrinsic and essentially perfectly symmetry-related probes has this built-in limitation. One way around this will be to engineer probes such as aromatic nitrile-containing amino acids into the RC at symmetry-related positions using amber suppression.[18] For example, in preliminary work, we have found the *o*-CN-phenylalanine can be incorporated close to H_L, and structural characterization demonstrates a single orientation for the −CN IR probe (J. Weaver and S.G. Boxer, to be published). This strategy should produce a more comprehensive mapping of electrostatic field differences on the L- and M-sides.

In contrast with the Bchls, the difference in frequencies are as large as 30 cm^{-1} for H_L versus H_M, where the larger shifts reflect the strong electrostatic fields arising from H-bonding interactions. Because of the large values of the difference dipoles, shifts of 30 cm^{-1} correspond to a difference in the electric field of 10*f* MV/cm for the 9-keto mode and below 15*f* MV/cm for the 2-acetyl mode. While not large in comparison to the effects associated with strong short hydrogen bonds,[25,36] a field difference of this magnitude could be energetically significant when considering the stabilization of long-range charge transfer, and in the present case, could be a significant determinant of the ∼65:1 preference for electron transfer along the L-branch, which would require the primary intermediate ($P^+H_L^-$) to be ∼2.5 kcal mol^{-1} more stable than the alternative ($P^+H_M^-$). The larger electrostatic field on H_L's 9-keto cannot directly explain the preference for L-branch ET because electrostatic stabilization of H_L^- will depend on the field on all regions of H_L where the transferred charge can delocalize. Nevertheless, the order of magnitude of this measured field difference (10*f* MV/cm), the dipole associated with charge transfer (2−10 D), and the energetic preference (2.5 kcal mol^{-1}) are all roughly consistent by the equation $\Delta U = \Delta\vec{F}\cdot\Delta\vec{\mu}$ (note that 1 MV/cm ≃ 0.048 kcal mol^{-1} D^{-1}).

In summary, the data in Table 2 are consistent with the possibility that H_L^- can be stabilized over H_M^- by a combination of a standard-strength hydrogen-bond (from Glu L104) and a global electric field effect that renders the environment surrounding H_L an effectively "more polar solvent" than the analogous region surrounding H_M. This hypothesis could be further examined by computationally examining the change in dipole on the 9-keto group of BPhe a upon one-electron reduction, to determine the energetic difference that would accompany the electrostatic field difference at this position. This study is an example of how new approaches, such as the vibrational Stark effect, can shed light on long-standing questions about charge transfer in reaction centers, and in protein biophysics more generally.

■ ASSOCIATED CONTENT

Supporting Information

The Supporting Information is available free of charge on the ACS Publications website at DOI: 10.1021/acs.jpcb.8b11458.

FTIR and Stark spectra of plant pigments; vibrational frequencies of isolated chromophores in different organic solvents; and MD parameters and calculated electric fields for chromophores (PDF)

DOI: 10.1021/acs.jpcb.8b11458
J. Phys. Chem. B 2019, 123, 1527−1536

AUTHOR INFORMATION

Corresponding Author

*E-mail: sboxer@stanford.edu.

ORCID

Steven G. Boxer: 0000-0001-9167-4286

Present Addresses

†Late Stage Pharmaceutical Development, Genentech Inc., South San Francisco, California 94080, USA (M.S.).

‡Department of Chemistry, Johns Hopkins University, Remsen Hall Room 121, 3400 N. Charles Street, Baltimore, Maryland 21218, USA (S.D.F.).

Notes

The authors declare no competing financial interest.

ACKNOWLEDGMENTS

This paper is dedicated to the memory of Jacques Breton who pioneered the application of FTIR to understanding local interactions in the reaction center. M.S. was supported by a DFG Forschungsstipendium (Deutsche Forschungsgemeinschaft, Sa 2156/1--1). S.D.F. was supported by an NSF predoctoral fellowship program and a Stanford Bio-X interdisciplinary graduate fellowship. We greatly appreciate long-standing support for this work from the NSF Biophysics Program (MCB1408785).

REFERENCES

(1) Blankenship, R. E. *Molecular Mechanisms of Photosynthesis*; John Wiley & Sons, 2014.

(2) Ermler, U.; Fritzsch, G.; Buchanan, S. K.; Michel, H. Structure of the photosynthetic reaction centre from Rhodobacter sphaeroides at 2.65 å resolution: cofactors and protein-cofactor interactions. *Structure* **1994**, *2*, 925−936.

(3) Deisenhofer, J.; Epp, O.; Miki, K.; Huber, R.; Michel, H. X-ray structure analysis of a membrane protein complex. *J. Mol. Biol.* **1984**, *180*, 385−398.

(4) Kirmaier, C.; Holten, D. Primary Photochemistry of Reaction Centers from the Photosynthetic Purple Bacteria. *Photosynth. Res.* **1987**, *13*, 225−260.

(5) Breton, J.; Boullais, C.; Burie, J.-R.; Nabedryk, E.; Mioskowski, C. Binding Sites of Quinones in Photosynthetic Bacterial Reaction Centers Investigated by Light-Induced Ftir Difference Spectroscopy: Assignment of the Interactions of Each Carbonyl of Qa in Rhodobacter Sphaeroides Using Site-Specific 13c-Labeled Ubiquinone. *Biochemistry* **2002**, *33*, 14378−14386.

(6) Carter, B.; Boxer, S. G.; Holten, D.; Kirmaier, C. Trapping the P +BL−Initial Intermediate State of Charge Separation in Photosynthetic Reaction Centers fromRhodobacter capsulatus. *Biochemistry* **2009**, *48*, 2571−2573.

(7) Zhang, L. Y.; Friesner, R. A. Ab Initio Calculation of Electronic Coupling in the Photosynthetic Reaction Center. *Proc. Natl. Acad. Sci. U.S.A.* **1998**, *95*, 13603−13605.

(8) Steffen, M. A.; Lao, K.; Boxer, S. G. Dielectric Asymmetry in the Photosynthetic Reaction Center. *Science* **1994**, *264*, 810−816.

(9) Alden, R. G.; Parson, W. W.; Chu, Z. T.; Warshel, A. Calculations of Electrostatic Energies in Photosynthetic Reaction Centers. *J. Am. Chem. Soc.* **1995**, *117*, 12284−12298.

(10) Gunner, M. R.; Nicholls, A.; Honig, B. Electrostatic Potentials inRhodopseudomonas viridisReaction Centers: Implications for the Driving Force and Directionality of Electron Transfer. *J. Phys. Chem.* **1996**, *100*, 4277−4291.

(11) Kim, H.; Cho, M. Infrared Probes for Studying the Structure and Dynamics of Biomolecules. *Chem. Rev.* **2013**, *113*, 5817−5847.

(12) Waegele, M. M.; Culik, R. M.; Gai, F. Site-Specific Spectroscopic Reporters of the Local Electric Field, Hydration, Structure, and Dynamics of Biomolecules. *J. Phys. Chem. Lett.* **2011**, *2*, 2598−2609.

(13) Fafarman, A. T.; Boxer, S. G. Nitrile Bonds as Infrared Probes of Electrostatics in Ribonuclease S. *J. Phys. Chem. B* **2010**, *114*, 13536−13544.

(14) Fafarman, A. T.; Webb, L. J.; Chuang, J. I.; Boxer, S. G. Site-Specific Conversion of Cysteine Thiols into Thiocyanate Creates an Ir Probe for Electric Fields in Proteins. *J. Am. Chem. Soc.* **2006**, *128*, 13356−13357.

(15) Jo, H.; Culik, R. M.; Korendovych, I. V.; DeGrado, W. F.; Gai, F. Selective Incorporation of Nitrile-Based Infrared Probes into Proteins Via Cysteine Alkylation. *Biochemistry* **2010**, *49*, 10354−10356.

(16) Fafarman, A. T. Quantitative Measurements of Electrostatic Fields in Proteins Using Vibrational Probes. Ph.D. Thesis, Stanford University, 2010.

(17) Chuang, J. Understanding Unidirectional Electron Transfer in the Photosynthetic Reaction Center Using Protein Engineering. Ph.D. Thesis, Stanford University, 2007.

(18) Weaver, J. B.; Boxer, S. G. Genetic Code Expansion in Rhodobacter Sphaeroides to Incorporate Noncanonical Amino Acids into Photosynthetic Reaction Centers. *ACS Synth. Biol.* **2018**, *7*, 1618−1628.

(19) Konar, A.; Sechrist, R.; Song, Y.; Policht, V. R.; Laible, P. D.; Bocian, D. F.; Holten, D.; Kirmaier, C.; Ogilvie, J. P. Electronic Interactions in the Bacterial Reaction Center Revealed by Two-Color 2d Electronic Spectroscopy. *J. Phys. Chem. Lett.* **2018**, *9*, 5219−5225.

(20) Ma, F.; Romero, E.; Jones, M. R.; Novoderezhkin, V. I.; van Grondelle, R. Vibronic Coherence in the Charge Separation Process of the Rhodobacter Sphaeroides Reaction Center. *J. Phys. Chem. Lett.* **2018**, *9*, 1827−1832.

(21) Mantele, W. G.; Wollenweber, A. M.; Nabedryk, E.; Breton, J. Infrared Spectroelectrochemistry of Bacteriochlorophylls and Bacteriopheophytins: Implications for the Binding of the Pigments in the Reaction Center from Photosynthetic Bacteria. *Proc. Natl. Acad. Sci. U.S.A.* **1988**, *85*, 8468−8472.

(22) Kirmaier, C.; Laible, P. D.; Czarnecki, K.; Hata, A. N.; Hanson, D. K.; Bocian, D. F.; Holten, D. Comparison of M-Side Electron Transfer inRb.sphaeroidesandRb.capsulatusReaction Centers. *J. Phys. Chem. B* **2002**, *106*, 1799−1808.

(23) Mattioli, T. A.; Williams, J. C.; Allen, J. P.; Robert, B. Changes in primary donor hydrogen-bonding interactions in mutant reaction centers from Rhodobacter sphaeroides : identification of the vibrational frequencies of all the conjugated carbonyl groups. *Biochemistry* **2002**, *33*, 1636−1643.

(24) Suydam, I. T.; Boxer, S. G. Vibrational Stark Effects Calibrate the Sensitivity of Vibrational Probes for Electric Fields in Proteins. *Biochemistry* **2003**, *42*, 12050−12055.

(25) Fried, S. D.; Boxer, S. G. Measuring Electric Fields and Noncovalent Interactions Using the Vibrational Stark Effect. *Acc. Chem. Res.* **2015**, *48*, 998−1006.

(26) Laible, P. D.; Kirmaier, C.; Udawatte, C. S. M.; Hofman, S. J.; Holten, D.; Hanson, D. K. Quinone Reduction via Secondary B-Branch Electron Transfer in Mutant Bacterial Reaction Centers. *Biochemistry* **2003**, *42*, 1718−1730.

(27) Scheer, H. *Chlorophylls*; CRC Press LLC, 1991.

(28) Omata, T.; Murata, N. Preparation of Chlorophyll a, Chlorophyll B and Bacteriochlorophyll a by Column Chromatography with Deae-Sepharose Cl-6b and Sepharose Cl-6b. *Plant Cell Physiol.* **1983**, *24*, 1093−1100.

(29) Andrews, S. S.; Boxer, S. G. A Liquid Nitrogen Immersion Cryostat for Optical Measurements. *Rev. Sci. Instrum.* **2000**, *71*, 3567−3569.

(30) Andrews, S. S.; Boxer, S. G. Vibrational Stark Effects of Nitriles I. Methods and Experimental Results. *J. Phys. Chem. A* **2000**, *104*, 11853−11863.

(31) Bublitz, G. U.; Boxer, S. G. Stark Spectroscopy: Applications in Chemistry, Biology, and Materials Science. *Annu. Rev. Phys. Chem.* **1997**, *48*, 213−242.

DOI: 10.1021/acs.jpcb.8b11458
J. Phys. Chem. B 2019, 123, 1527−1536

(32) *Spectfit*, Version 2.0, http://www.smoldyn.org/andrews/software.html.
(33) Zhang, L.; Silva, D.-A.; Yan, Y.; Huang, X. Force Field Development for Cofactors in the Photosystem Ii. *J. Comput. Chem.* **2012**, *33*, 1969−1980.
(34) Ceccarelli, M.; Procacci, P.; Marchi, M. Anab initio force field for the cofactors of bacterial photosynthesis. *J. Comput. Chem.* **2002**, *24*, 129−142.
(35) Caleman, C.; van Maaren, P. J.; Hong, M.; Hub, J. S.; Costa, L. T.; van der Spoel, D. Force Field Benchmark of Organic Liquids: Density, Enthalpy of Vaporization, Heat Capacities, Surface Tension, Isothermal Compressibility, Volumetric Expansion Coefficient, and Dielectric Constant. *J. Chem. Theory Comput.* **2011**, *8*, 61−74.
(36) Fried, S. D.; Bagchi, S.; Boxer, S. G. Measuring Electrostatic Fields in Both Hydrogen-Bonding and Non-Hydrogen-Bonding Environments Using Carbonyl Vibrational Probes. *J. Am. Chem. Soc.* **2013**, *135*, 11181−11192.
(37) Blankenship, R. E.; Madigan, M. T.; Bauer, C. E. *Anoxygenic Photosynthetic Bacteria*; Springer Science & Business Media, 2006; Vol. 2.
(38) Saggu, M.; Levinson, N. M.; Boxer, S. G. Experimental Quantification of Electrostatics in X-H···π Hydrogen Bonds. *J. Am. Chem. Soc.* **2012**, *134*, 18986−18997.
(39) Park, E. S.; Boxer, S. G. Origins of the Sensitivity of Molecular Vibrations to Electric Fields: Carbonyl and Nitrosyl Stretches in Model Compounds and Proteins. *J. Phys. Chem. B* **2002**, *106*, 5800−5806.
(40) Breton, J.; Burie, J.-R.; Berthomieu, C.; Berger, G.; Nabedryk, E. The Binding Sites of Quinones in Photosynthetic Bacterial Reaction Centers Investigated by Light-Induced FTIR Difference Spectroscopy: Assignment of the QA Vibrations in Rhodobacter sphaeroides Using 18O- or 13C-Labeled Ubiquinones and Vitamin K1. *Biochemistry* **2002**, *33*, 4953−4965.
(41) Bellamy, L. J.; Williams, R. L. Infra-red spectra and solvent effects. Part 2.-Carbonyl absorptions. *Trans. Faraday Soc.* **1959**, *55*, 14−18.
(42) Schneider, S. H.; Kratochvil, H. T.; Zanni, M. T.; Boxer, S. G. Solvent-Independent Anharmonicity for Carbonyl Oscillators. *J. Phys. Chem. B* **2017**, *121*, 2331−2338.
(43) Koepke, J.; Krammer, E.-M.; Klingen, A. R.; Sebban, P.; Ullmann, G. M.; Fritzsch, G. Ph Modulates the Quinone Position in the Photosynthetic Reaction Center from Rhodobacter Sphaeroides in the Neutral and Charge Separated States. *J. Mol. Biol.* **2007**, *371*, 396−409.
(44) Heller, B.; Holten, D.; Kirmaier, C. Control of electron transfer between the L- and M-sides of photosynthetic reaction centers. *Science* **1995**, *269*, 940−945.
(45) Breton, J.; Bibikova, M.; Oesterhelt, D.; Nabedryk, E. Conformational Heterogeneity of the Bacteriopheophytin Electron Acceptor HA in Reaction Centers from Rhodopseudomonas viridis Revealed by Fourier Transform Infrared Spectroscopy and Site-Directed Mutagenesis. *Biochemistry* **1999**, *38*, 11541−11552.
(46) Robert, B. Resonance Raman Studies of Bacterial Reaction Centers. *Biochim. Biophys. Acta* **1990**, *1017*, 99−111.
(47) Frolov, D.; Gall, A.; Lutz, M.; Robert, B. Structural Asymmetry of Bacterial Reaction Centers: A Qy Resonant Raman Study of the Monomer Bacteriochlorophylls. *J. Phys. Chem. A* **2002**, *106*, 3605−3613.
(48) Fried, S. D.; Bagchi, S.; Boxer, S. G. Extreme Electric Fields Power Catalysis in the Active Site of Ketosteroid Isomerase. *Science* **2014**, *346*, 1510.
(49) Fried, S. D.; Boxer, S. G. Electric Fields and Enzyme Catalysis. *Annu. Rev. Biochem.* **2017**, *86*, 387−415.
(50) Mattioli, T. A.; Lin, X.; Allen, J. P.; Williams, J. C. Correlation between Multiple Hydrogen Bonding and Alteration of the Oxidation Potential of the Bacteriochlorophyll Dimer of Reaction Centers from Rhodobacter Sphaeroides. *Biochemistry* **2002**, *34*, 6142−6152.
(51) Mattioli, T. A.; Hoffmann, A.; Robert, B.; Schrader, B.; Lutz, M. Primary Donor Structure and Interactions in Bacterial Reaction Centers from near-Infrared Fourier Transform Resonance Raman Spectroscopy. *Biochemistry* **2002**, *30*, 4648−4654.
(52) Palaniappan, V.; Martin, P. C.; Chynwat, V.; Frank, H. A.; Bocian, D. F. Comprehensive Resonance Raman Study of Photosynthetic Reaction Centers from Rhodobacter Sphaeroides. Implications for Pigment Structure and Pigment-Protein Interactions. *J. Am. Chem. Soc.* **1993**, *115*, 12035−12049.
(53) Robert, B.; Lutz, M. Proteic Events Following Charge Separation in the Bacterial Reaction Center: Resonance Raman Spectroscopy. *Biochemistry* **2002**, *27*, 5108−5114.
(54) Chen, L.; Kirmaier, C.; Holten, D.; Bocian, D. F. Resonance Raman Characterization of Rhodobacter Capsulatus Reaction Centers with Lysine Mutations near the Accessory Bacteriochlorophylls. *Photosynth. Res.* **2005**, *83*, 35−43.
(55) Ivancich, A.; Lutz, M.; Mattioli, T. A. Temperature-Dependent Behavior of Bacteriochlorophyll and Bacteriopheophytin in the Photosynthetic Reaction Center fromRhodobacter sphaeroides. *Biochemistry* **1997**, *36*, 3242−3253.
(56) Palaniappan, V.; Bocian, D. F. Resonance Raman Spectroscopic Evidence for Dielectric Asymmetry in Bacterial Photosynthetic Reaction Centers. *J. Am. Chem. Soc.* **1995**, *117*, 3647−3648.
(57) Hughes, J. M.; Hutter, M. C.; Reimers, J. R.; Hush, N. S. Modeling the Bacterial Photosynthetic Reaction Center. 4. The Structural, Electrochemical, and Hydrogen-Bonding Properties of 22 Mutants ofRhodobacter sphaeroides. *J. Am. Chem. Soc.* **2001**, *123*, 8550−8563.
(58) Moore, L. J.; Zhou, H.; Boxer, S. G. Excited-State Electronic Asymmetry of the Special Pair in Photosynthetic Reaction Center Mutants: Absorption and Stark Spectroscopy. *Biochemistry* **1999**, *38*, 11949−11960.

DOI: 10.1021/acs.jpcb.8b11458
J. Phys. Chem. B 2019, 123, 1527−1536

Supporting Information for

Local and Global Electric Field Asymmetry in Photosynthetic Reaction Centers

Miguel Saggu[†], Stephen D. Fried[‡], and Steven G. Boxer[*]

Department of Chemistry, Stanford University, Stanford, CA 94305-5080, USA

[*] To whom correspondence should be addressed: sboxer@stanford.edu

[†] Current address: Late Stage Pharmaceutical Development, Genentech Inc., South San Francisco, California 94080, USA

[‡] Current address: Department of Chemistry, Johns Hopkins University, Remsen Hall Room 121, 3400 N. Charles Street, Baltimore, Md. 21218

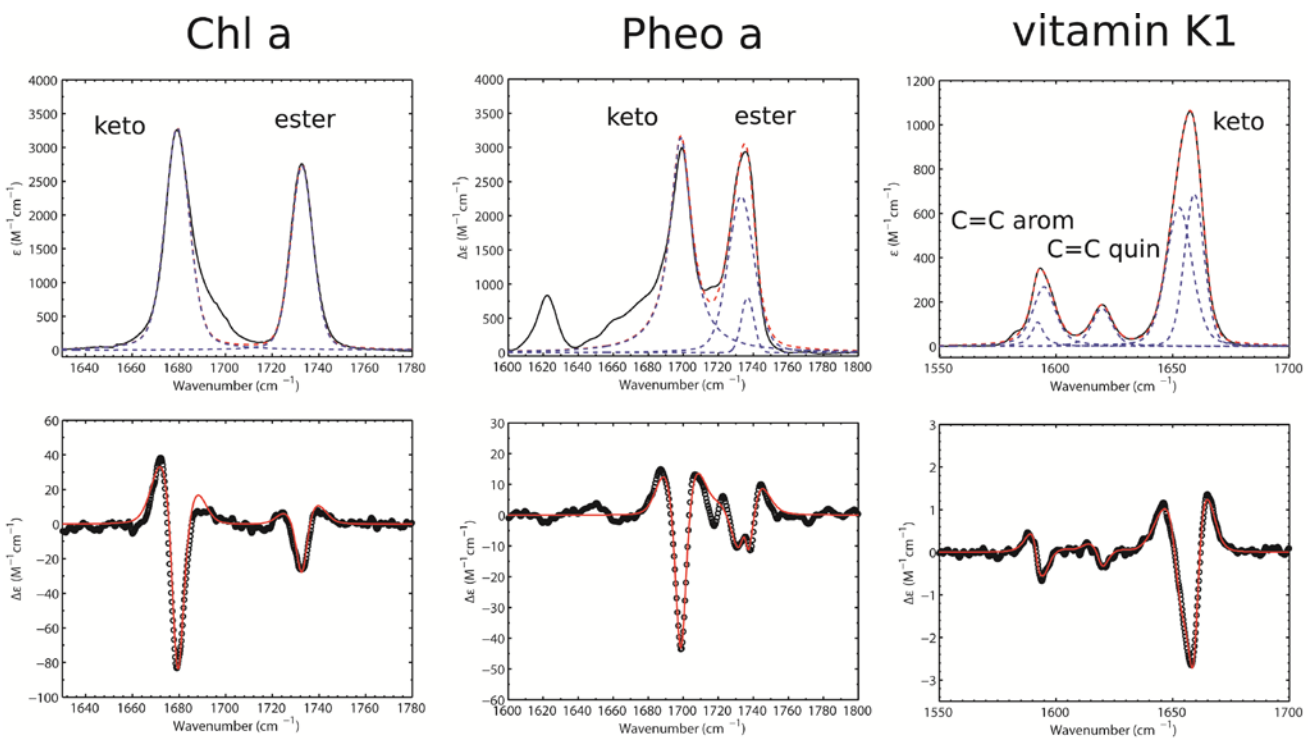

Figure S1 FTIR spectra in the carbonyl region (upper) and vibrational Stark spectra (lower) of photosynthetic chromophores at T = 77 K. 5 mM Chl *a* in 2-methyl-THF; 4.4 mM Phe *a* in 2-methyl-THF; 5 mM vitamin K1 in DCM/DCE. Vibrational Stark spectra are overlaid with best fits shown in red giving $|\Delta\vec{\mu}| \cdot f$ (see Table 1). Stark spectra are scaled to an external field of 1 MV/cm. ($\tilde{\nu}_{keto1}$ = 1659 cm^{-1}, $\varepsilon_{\max}$ = 690 M^{-1}cm^{-1}; $\tilde{\nu}_{keto2}$ = 1653 cm^{-1}, $\varepsilon_{\max}$ = 630 M^{-1}cm^{-1}; $\tilde{\nu}_{C=C-quin}$ = 1620 cm^{-1}, $\varepsilon_{\max}$ = 170 M^{-1}cm^{-1}; $\tilde{\nu}_{C=C-arom}$ = 1595 cm^{-1}, $\varepsilon_{\max}$ = 270 M^{-1}cm^{-1}; $\tilde{\nu}_{C=C-arom-sideband}$ = 1592 cm^{-1}, $\varepsilon_{\max}$ = 110 M^{-1}cm^{-1}).

Table S1. Measured vibrational frequencies in cm^{-1} of the chromophores dissolved in various solvents. Note that BChl a and Chl a have 6 equivalents of pyridine added to keep them monomeric.

	BChl a			Chl a		BPhe a		
	ester	9-keto	acetyl	ester	9-keto	ester	9-keto	acetyl
cyclohexane	1737.6	1698.4	1652.8	1741.2	1705.4	-	1712	1674
Et2O	1740	1692	1661	1740.7	1701.2	-	1708	1674
THF	1737.6	1686	1653.8	1738	1695.3	-	1701	1669
pyridine	1732.6	1675	1665	-	-	-	-	-
ACN	1734.1	1678	1669	1735	1684.6	1733	1691	1666
CHCl3	1730.4	1676	1661	1731	1679.1	1736	1698	1668
DCM	1732.8	1674	1661	1733.4	1682.9	1737	1695	1670
DMSO	1730.2	1668	1647	1732.3	1681	-	-	-

Table S2. Calculated electric fields for vibrations of pigments dissolved in various solvents. Solvent fields reported as the average over the trajectory along with correlation-adjusted error (all in units of MV/cm). Standard deviations for each electric field entry are given as well (also in units of MV/cm). Abbreviations: CXH, cyclohexane; THF, tetrahydrofuran; DMF, dimethyl formamide; DMSO, dimethyl sulfoxide; DCM, dichloromethane; ACN, acetonitrile.

Chlorophyll

	9-keto			10a-ester			7c-ester		
	field	error	std. dev	field	error	std. dev	field	error	std. dev
CXH	-0.012434	0.023656	0.72541	0.075310	0.027132	0.70143	0.032271	0.062061	0.71385
ether	-11.818	0.39350	5.0922	-5.4610	0.34158	5.3904	-7.0494	0.78493	6.7588
THF	-16.580	0.26158	6.4229	-10.084	0.59645	7.0090	-11.644	0.31779	7.6801
pyridine	-21.362	0.49583	7.9482	-15.284	0.49193	9.2073	-17.616	0.56169	9.4654
acetone	-22.868	0.57787	8.3278	-12.547	0.54200	8.9251	-18.338	1.3510	10.084
DMF	-28.724	0.38922	8.6746	-17.273	1.1156	9.6087	-22.279	0.71904	10.537
DMSO	-27.285	1.0229	8.8723	-17.997	0.93743	9.8659	-20.856	0.62347	10.534
chloroform	-28.852	0.72160	13.438	-21.072	0.70419	13.608	-26.855	0.65203	13.062
DCM	-27.041	0.39646	12.350	-20.774	0.43520	12.906	-26.678	1.3158	12.822
acetonitrile	-24.712	0.098353	9.8358	-19.640	0.38013	10.762	-21.354	0.90245	11.142

Pheophytin

	9-keto			10a-ester			7c-ester		
	field	error	std. dev	field	error	std. dev	field	error	std. dev
CXH	0.047606	0.025706	0.71109	0.034830	0.033795	0.62259	0.090113	0.039419	0.72088
ether	-6.4665	0.33002	5.8862	-1.7574	0.40197	5.1855	-6.7318	0.49002	6.3743
THF	-12.832	0.20629	6.7143	-4.3022	0.44078	6.9236	-12.439	0.65038	8.2837
Pyridine	-20.898	0.32508	8.4505	-7.9185	0.86906	8.9438	-18.562	0.80535	9.6327
DMSO	-20.434	0.53520	10.084	-20.093	2.5480	11.855	-17.036	1.1437	11.874
chloroform	-29.231	0.64589	13.309	-13.731	1.5653	13.488	-20.098	1.5151	14.004
DCM	-26.710	0.51875	12.404	-18.621	1.1359	13.256	-22.132	1.6584	13.734

Bacteriochlorophyll

	9-keto			10a-ester			7c-ester			acetyl		
	field	error	std. dev	field	error	std. dev	field	error	std. dev	field	error	std. dev
CXH	0.054013	0.022260	0.69875	0.073631	0.048481	0.67948	-0.007154	0.022105	0.69095	0.055382	0.037273	0.74923
ether	-10.113	0.84137	7.1605	-5.9446	0.21272	6.0914	-6.7980	0.60884	6.6941	-12.368	0.82158	7.9643
THF	-12.363	0.89569	10.427	-8.5045	0.95322	9.1485	-11.519	0.43789	8.1643	-19.239	0.90590	12.899
pyridine	-17.049	1.9349	16.569	-10.148	1.4831	14.231	-14.761	1.2551	12.730	-23.137	1.5836	16.180
acetone	-18.999	1.4787	15.030	-10.382	1.3241	13.699	-14.072	1.4591	14.119	-20.820	2.0771	20.736
ACN	-23.520	0.44058	12.601	-19.827	0.36622	12.152	-18.348	1.1800	15.513	-29.172	0.33759	13.199
DMSO	-26.088	2.9826	17.885	-19.640	2.3330	13.844	-11.327	1.1909	19.446	-30.964	4.3024	22.652
$CHCl_3$	-22.038	2.7595	24.086	-16.197	1.0916	18.154	-19.557	1.8361	17.880	-22.224	0.92275	15.643
DCM	-24.931	1.8336	17.239	-19.665	1.1948	15.125	-23.876	1.7767	18.048	-22.875	1.9388	16.199

Bacteriopheophytin

	9-keto			10a-ester			7c-ester			acetyl		
	field	mean	std. dev	field	mean	std. dev	field	mean	std. dev	field	mean	std. dev
CXH	0.015509	0.018469	0.66740	0.036457	0.013899	0.66987	-0.03076	0.017604	0.65336	-0.05899	0.025168	0.70917
ether	-7.3524	0.43306	5.3846	-5.7188	0.71410	5.9331	-6.2979	1.0797	6.8569	-13.996	0.19008	7.1971
THF	-11.429	0.11398	6.8194	-10.004	0.50608	7.7609	-9.6155	0.61233	8.2505	-22.816	0.28441	9.0821
pyridine	-21.772	0.78459	8.7748	-12.399	0.89186	9.2820	-14.945	1.1118	10.470	-26.907	0.73261	10.229
ACN	-21.191	0.33321	10.192	-19.638	0.56134	11.132	-18.530	1.7515	11.383	-30.103	0.15866	10.856
DMSO	-21.179	0.31720	9.7194	-22.270	1.1183	10.753	-18.727	1.5534	11.693	-43.764	0.78170	12.168
$CHCl_3$	-26.903	0.43056	13.582	-18.949	2.4155	14.421	-22.254	1.1588	13.977	-22.497	0.73714	12.591
DCM	-24.642	0.93726	12.710	-21.280	0.70513	13.121	-21.582	0.72130	12.767	-25.124	0.16564	11.438

Parameters for Bacteriochlorophyll (BCL) and Bacteriopheophytin (BPH).
Additional lines to the files cofactors.hdb and cofactors.rtp from Zhang's amber03.ff (GROMACS format). For digital versions, please e-mail Stephen Fried (sdfried@gmail.com).

Added to cofactors.hdb

```
BCL     37
3       4       H7B     C7B     C6B     C3B
3       4       HMB     CMB     C2B     C1B
1       1       HHB     CHB     C1B     C4A
1       1       HHC     CHC     C4B     C1C
3       4       H5C     C5C     C2CX    C1C
3       4       HBC     CBC     CAC     C3CX
2       6       HAC     CAC     CBC     C3CX
1       5       H2CX    C2CX    C1C     C3CX    C5C
1       5       H3CX    C3CX    C4C     C2CX    CAC
1       1       HHD     CHD     C4C     C1D
3       4       HMD     CMD     C2D     C1D
1       5       HBD     CBD     CHA     CAD     CGD
3       4       HED     CED     O2D     CGD
1       5       H3A     C3A     C4A     C2A     CMA
3       4       HMA     CMA     C3A     C2A
1       5       H2A     C2A     C1A     C3A     CAA
2       6       HAA     CAA     C2A     CBA
2       6       HBA     CBA     CGA     CAA
2       6       H1      C1      O2A     C2
1       1       H2      C2      C1      C3
3       4       H4      C4      C3      C2
2       6       H5      C5      C3      C6
2       6       H6      C6      C5      C7
2       6       H7      C7      C6      C8
1       5       H8      C8      C7      C9      C10
3       4       H9      C9      C8      C7
2       6       H10     C10     C8      C11
2       6       H11     C11     C10     C12
2       6       H12     C12     C11     C13
1       5       H13     C13     C12     C14     C15
3       4       H14     C14     C13     C12
2       6       H15     C15     C13     C16
2       6       H16     C16     C15     C17
2       6       H17     C17     C16     C18
1       5       H18     C18     C17     C19     C20
3       4       H19     C19     C18     C17
3       4       H20     C20     C18     C17
BPH     39
3       4       H7B     C7B     C6B     C3B
3       4       HMB     CMB     C2B     C1B
1       1       HHB     CHB     C1B     C4A
1       1       HHC     CHC     C4B     C1C
3       4       H5C     C5C     C2CX    C1C
3       4       HBC     CBC     CAC     C3CX
2       6       HAC     CAC     CBC     C3CX
1       5       H2CX    C2CX    C1C     C3CX    C5C
1       5       H3CX    C3CX    C4C     C2CX    CAC
1       1       HHD     CHD     C4C     C1D
3       4       HMD     CMD     C2D     C1D
1       5       HBD     CBD     CHA     CAD     CGD
```

```
3       4       HED     CED     O2D     CGD
1       5       H3A     C3A     C4A     C2A     CMA
3       4       HMA     CMA     C3A     C2A
1       5       H2A     C2A     C1A     C3A     CAA
2       6       HAA     CAA     C2A     CBA
2       6       HBA     CBA     CGA     CAA
2       6       H1      C1      O2A     C2
1       1       H2      C2      C1      C3
3       4       H4      C4      C3      C2
2       6       H5      C5      C3      C6
2       6       H6      C6      C5      C7
2       6       H7      C7      C6      C8
1       5       H8      C8      C7      C9      C10
3       4       H9      C9      C8      C7
2       6       H10     C10     C8      C11
2       6       H11     C11     C10     C12
2       6       H12     C12     C11     C13
1       5       H13     C13     C12     C14     C15
3       4       H14     C14     C13     C12
2       6       H15     C15     C13     C16
2       6       H16     C16     C15     C17
2       6       H17     C17     C16     C18
1       5       H18     C18     C17     C19     C20
3       4       H19     C19     C18     C17
3       4       H20     C20     C18     C17
1       1       HB      NB      C1B     C4B
1       1       HD      ND      C1D     C4D
```

Added to cofactors.rtp

```
[ BCL ]
 [ atoms ]
   MG      mgc       1.140797       1
   CHA     csb       0.073563       2
   CHB     cab      -0.530666       3
   CHC     cab      -0.293706       4
   CHD     cab      -0.381654       5
   NA      ns       -0.401782       6
   C1A     ccs      -0.027935       7
   C2A     ct1      -0.100818       8
   C3A     ct1       0.259931       9
   C4A     ccs       0.273045      10
   CMA     ct3      -0.347802      11
   CAA     ct2      -0.066561      12
   CBA     ct2      -0.370595      13
   CGA     c2a       0.722546      14
   O1A     o2c      -0.577588      15
   O2A     o1c      -0.390978      16
   NB      nmh      -0.522883      17
   C1B     crb       0.290613      18
   C2B     cbb       0.056235      19
   C3B     cbb      -0.059508      20
   C4B     cnb       0.201631      21
   CMB     ct3      -0.196671      22
   C6B     c2e       0.6950        23
   C7B     ct3      -0.3920        24
   NC      ns       -0.500171      25
   C1C     ccs       0.173876      26
   C2CX    ct1       0.063127      27
```

C3CX	ct1	-0.155844	28
C4C	ccs	0.313793	29
C5C	ct3	-0.242247	30
CAC	ct2	0.190617	31
CBC	ct3	-0.128605	32
ND	nmh	-0.496512	33
C1D	cpb	0.199807	34
C2D	cbb	0.067465	35
C3D	cbb	-0.256041	36
C4D	cqb	0.145335	37
CMD	ct3	-0.257732	38
CAD	c2k	0.711103	39
OBD	o2c	-0.57472	40
CBD	ct1	-0.635795	41
CGD	c2a	0.907866	42
O1D	o2c	-0.603021	43
O2D	o1c	-0.381813	44
CED	ct3	0.011315	45
C1	ct2	0.183261	46
C2	cqq	-0.404524	47
C3	cq2	0.231494	48
C4	ct3	-0.171786	49
C5	ct2	-0.329157	50
C6	ct2	0.107607	51
C7	ct2	-0.097062	52
C8	ct1	0.223668	53
C9	ct3	-0.306973	54
C10	ct2	-0.096255	55
C11	ct2	0.050839	56
C12	ct2	-0.149838	57
C13	ct1	0.277566	58
C14	ct3	-0.306597	59
C15	ct2	-0.133326	60
C16	ct2	0.063751	61
C17	ct2	-0.174116	62
C18	ct1	0.431195	63
C19	ct3	-0.351586	64
C20	ct3	-0.351586	65
HHB	HA	0.18194	66
HHC	HA	0.147981	67
HHD	HA	0.220211	68
H2A	HC	0.11891	69
H3A	HC	0.009865	70
HMA1	HC	0.088879	71
HMA2	HC	0.088879	72
HMA3	HC	0.088879	73
HAA1	HC	0.074129	74
HAA2	HC	0.074129	75
HBA1	HC	0.123685	76
HBA2	HC	0.123685	77
HMB1	HC	0.069103	78
HMB2	HC	0.069103	79
HMB3	HC	0.069103	80
OB	o2c	-0.5370	81
H7B1	HC	0.075196	82
H7B2	HC	0.075196	83
H5C1	HC	0.07984	84
H5C2	HC	0.07984	85
H5C3	HC	0.07984	86

```
  HAC1    HC       -0.010598      87
  HAC2    HC       -0.010598      88
  HBC1    HC        0.029396      89
  HBC2    HC        0.029396      90
  HBC3    HC        0.029396      91
  HMD1    HC        0.084447      92
  HMD2    HC        0.084447      93
  HMD3    HC        0.084447      94
  HBD     HC        0.195581      95
  HED1    HC        0.069208      96
  HED2    HC        0.069208      97
  HED3    HC        0.069208      98
  H11     HC        0.067685      99
  H12     HC        0.067685     100
  H2      HA        0.189077     101
  H41     HC        0.059658     102
  H42     HC        0.059658     103
  H43     HC        0.059658     104
  H51     HC        0.095476     105
  H52     HC        0.095476     106
  H61     HC        0.000653     107
  H62     HC        0.000653     108
  H71     HC        0.012281     109
  H72     HC        0.012281     110
  H8      HC       -0.018459     111
  H91     HC        0.063458     112
  H92     HC        0.063458     113
  H93     HC        0.063458     114
  H101    HC        0.017558     115
  H102    HC        0.017558     116
  H111    HC        0.003086     117
  H112    HC        0.003086     118
  H121    HC        0.028404     119
  H122    HC        0.028404     120
  H13     HC       -0.028733     121
  H141    HC        0.059372     122
  H142    HC        0.059372     123
  H143    HC        0.059372     124
  H151    HC        0.028933     125
  H152    HC        0.028933     126
  H161    HC       -0.009013     127
  H162    HC       -0.009013     128
  H171    HC        0.028341     129
  H172    HC        0.028341     130
  H18     HC       -0.060142     131
  H191    HC        0.06933      132
  H192    HC        0.06933      133
  H193    HC        0.06933      134
  H201    HC        0.06933      135
  H202    HC        0.06933      136
  H203    HC        0.06933      137
  H2CX    HC        0.063127     138
  H3CX    HC       -0.155844     139
  H7B3    HC        0.075196      140

[ bonds ]
    C1B   C2B
    C2B   C3B
    C3B   C4B
```

```
C4B    NB
 NB   C1B
C2B   CMB
C3B   C6B
C6B   OB
C6B   C7B
C4B   CHC
CHC   C1C
C1C   C2CX
C2CX  H2CX
C2CX  C3CX
C3CX  H3CX
C3CX  C4C
C4C    NC
 NC   C1C
C2CX  C5C
C3CX  CAC
CAC   CBC
C4C   CHD
CHD   C1D
C1D   C2D
C2D   C3D
C3D   C4D
C4D    ND
ND    C1D
C2D   CMD
C3D   CAD
CAD   CBD
CBD   CHA
CHA   C4D
CAD   OBD
CBD   CGD
CGD   O1D
CGD   O2D
O2D   CED
CHA   C1A
C1A   C2A
C2A   C3A
C3A   C4A
C4A    NA
 NA   C1A
C4A   CHB
CHB   C1B
C3A   CMA
C2A   CAA
CAA   CBA
CBA   CGA
CGA   O1A
CGA   O2A
O2A    C1
 C1    C2
 C2    C3
 C3    C4
 C3    C5
 C5    C6
 C6    C7
 C7    C8
 C8    C9
 C8   C10
```

```
C10  C11
C11  C12
C12  C13
C13  C14
C13  C15
C15  C16
C16  C17
C17  C18
C18  C19
C18  C20
CHB  HHB
CHC  HHC
CHD  HHD
C2A  H2A
C3A  H3A
CMA HMA1
CMA HMA2
CMA HMA3
CAA HAA1
CAA HAA2
CBA HBA1
CBA HBA2
 NB   MG
CMB HMB1
CMB HMB2
CMB HMB3
C7B H7B1
C7B H7B2
C7B H7B3
C5C H5C1
C5C H5C2
C5C H5C3
CAC HAC1
CAC HAC2
CBC HBC1
CBC HBC2
CBC HBC3
 ND   MG
CMD HMD1
CMD HMD2
CMD HMD3
CBD  HBD
CED HED1
CED HED2
CED HED3
 C1  H11
 C1  H12
 C2   H2
 C4  H41
 C4  H42
 C4  H43
 C5  H51
 C5  H52
 C6  H61
 C6  H62
 C7  H71
 C7  H72
 C8   H8
 C9  H91
```

```
      C9  H92
      C9  H93
     C10 H101
     C10 H102
     C11 H111
     C11 H112
     C12 H121
     C12 H122
     C13  H13
     C14 H141
     C14 H142
     C14 H143
     C15 H151
     C15 H152
     C16 H161
     C16 H162
     C17 H171
     C17 H172
     C18  H18
     C19 H191
     C19 H192
     C19 H193
     C20 H201
     C20 H202
     C20 H203
     MG  NC
     MG  NA

 [ angles ]
;  i     j    k         th0       cth
   NA    MG   NC       176.1     418.400
   NB    MG   ND       178.9     418.400


 [ impropers ]
    C3    C1    C2    H2
    C2    C5    C3    C4
   O2A   CBA   CGA   O1A
   C2A   CHA   C1A    NA
   C3A   CHB   C4A    NA
   C1B   C4A   CHB   HHB
   C4B   C2B   C3B   C6B
   C3B   CHC   C4B    NB
   C2B   CHB   C1B    NB
   CMB   C3B   C2B   C1B
   CBD   C4D   CHA   C1A
   CBD   O2D   CGD   O1D
   CBD   C3D   CAD   OBD
   CAD   C4D   C3D   C2D
   C3D   CHA   C4D    ND
   C2D   CHD   C1D    ND
   CMD   C1D   C2D   C3D
   C1D   C4C   CHD   HHD
   C3CX  CHD   C4C    NC
   CAC   C2CX  C3CX  C4C
   C2CX  CHC   C1C    NC
   C5C   C1C   C2CX  C3CX
   C1C   C4B   CHC   HHC
```

```
[ BPH ]
 [ atoms ]
   C19     ct3        -0.35398      1
  H191     HC          0.07347      2
  H192     HC          0.07347      3
  H193     HC          0.07347      4
   C18     ct1         0.38934      5
   C20     ct3        -0.35398      6
  H201     HC          0.07347      7
  H202     HC          0.07347      8
  H203     HC          0.07347      9
   H18     HC         -0.04653     10
   C17     ct2        -0.15263     11
  H171     HC          0.03273     12
  H172     HC          0.03273     13
   C16     ct2        -0.00189     14
  H161     HC          0.00974     15
  H162     HC          0.00974     16
   C15     ct2        -0.17051     17
  H151     HC          0.03664     18
  H152     HC          0.03664     19
   C13     ct1         0.38169     20
   C14     ct3        -0.33615     21
  H141     HC          0.07019     22
  H142     HC          0.07019     23
  H143     HC          0.07019     24
   H13     HC         -0.05480     25
   C12     ct2        -0.22819     26
  H121     HC          0.02074     27
  H122     HC          0.02074     28
   C11     ct2         0.29696     29
  H111     HC         -0.08535     30
  H112     HC         -0.08535     31
   C10     ct2        -0.16967     32
  H101     HC          0.01763     33
  H102     HC          0.01763     34
    C8     ct1         0.38123     35
    C9     ct3        -0.31498     36
   H91     HC          0.05864     37
   H92     HC          0.05864     38
   H93     HC          0.05864     39
    H8     HC         -0.06230     40
    C7     ct2        -0.27691     41
   H71     HC          0.05395     42
   H72     HC          0.05395     43
    C6     ct2         0.23442     44
   H61     HC         -0.01317     45
   H62     HC         -0.01317     46
    C5     ct2        -0.33480     47
   H51     HC          0.08985     48
   H52     HC          0.08985     49
    C3     cq2         0.21940     50
    C4     ct3        -0.23434     51
   H41     HC          0.08186     52
   H42     HC          0.08186     53
   H43     HC          0.08186     54
    C2     cqq        -0.46505     55
    H2     HA          0.18728     56
    C1     ct2         0.29369     57
```

H11	HC	0.03319	58
H12	HC	0.03319	59
O2A	o1c	-0.48504	60
CGA	c2a	0.90692	61
O1A	o2c	-0.59685	62
CBA	ct2	-0.46156	63
HBA1	HC	0.12241	64
HBA2	HC	0.12241	65
CAA	ct2	-0.04519	66
HAA1	HC	0.03991	67
HAA2	HC	0.03991	68
C2A	ct1	0.17580	69
H2A	HC	0.05578	70
C3A	ct1	0.15276	71
CMA	ct3	-0.36836	72
HMA1	HC	0.09451	73
HMA2	HC	0.09451	74
HMA3	HC	0.09451	75
H3A	HC	0.01996	76
C4A	ccs	0.25138	77
CHB	cab	-0.40864	78
C1B	crb	0.12523	79
NB	nh	-0.09693	80
C4B	cnb	0.04385	81
C3B	cbb	-0.02531	82
C2B	cbb	0.09630	83
CMB	ct3	-0.24283	84
HMB1	HC	0.08822	85
HMB2	HC	0.08822	86
HMB3	HC	0.08822	87
C6B	c2e	0.6950	88
C7B	ct3	-0.3920	89
OB	o2c	-0.5370	90
H7B1	HC	0.075196	91
H7B2	HC	0.075196	92
HB	hn	0.16372	93
HHB	HA	0.14909	94
NA	ns	-0.28377	95
C1A	ccs	-0.11228	96
CHA	csb	0.12976	97
C4D	cqb	0.01537	98
ND	nh	0.02972	99
HD	hn	0.08885	100
CBD	ct1	-0.67857	101
CGD	c2a	0.82970	102
O1D	o2c	-0.57388	103
O2D	o1c	-0.35614	104
CED	ct3	0.06662	105
HED1	HC	0.05534	106
HED2	HC	0.05534	107
HED3	HC	0.05534	108
HBD	HC	0.24601	109
CAD	c2k	0.75090	110
OBD	o2c	-0.58383	111
C3D	cbb	-0.29487	112
C2D	cbb	0.14152	113
CMD	ct3	-0.27550	114
HMD1	HC	0.09098	115
HMD2	HC	0.09098	116

```
 HMD3     HC          0.09098    117
  C1D     cpb        -0.01318    118
  CHD     cab        -0.26370    119
  HHD     HA          0.21030    120
  C4C     ccs         0.22486    121
  C3CX    ct1        -0.14940    122
  CAC     ct2         0.18449    123
  CBC     ct3        -0.10787    124
 HBC1     HC          0.02491    125
 HBC2     HC          0.02491    126
 HBC3     HC          0.02491    127
 HAC1     HC         -0.01274    128
 HAC2     HC         -0.01274    129
  C2CX    ct1         0.08674    130
  C5C     ct3        -0.28573    131
 H5C1     HC          0.08922    132
 H5C2     HC          0.08922    133
 H5C3     HC          0.08922    134
   NC     ns         -0.31971    135
  C1C     ccs         0.11298    136
  CHC     cab        -0.21525    137
  HHC     HA          0.13603    138
  H2CX    HC          0.08674    139
  H3CX    HC         -0.14940    140
 H7B3     HC        0.075196   141

[ bonds ]
  C19    H191
  C19    H192
  C19    H193
  C19     C18
  C18     C20
  C18     H18
  C18     C17
  C20    H201
  C20    H202
  C20    H203
  C17    H171
  C17    H172
  C17     C16
  C16    H161
  C16    H162
  C16     C15
  C15    H151
  C15    H152
  C15     C13
  C13     C14
  C13     H13
  C13     C12
  C14    H141
  C14    H142
  C14    H143
  C12    H121
  C12    H122
  C12     C11
  C11    H111
  C11    H112
  C11     C10
  C10    H101
```

C10 H102
C10 C8
C8 C9
C8 H8
C8 C7
C9 H91
C9 H92
C9 H93
C7 H71
C7 H72
C7 C6
C6 H61
C6 H62
C6 C5
C5 H51
C5 H52
C5 C3
C3 C4
C3 C2
C4 H41
C4 H42
C4 H43
C2 H2
C2 C1
C1 H11
C1 H12
C1 O2A
O2A CGA
CGA O1A
CGA CBA
CBA HBA1
CBA HBA2
CBA CAA
CAA HAA1
CAA HAA2
CAA C2A
C2A H2A
C2A C3A
C2A C1A
C3A CMA
C3A H3A
C3A C4A
CMA HMA1
CMA HMA2
CMA HMA3
C4A CHB
C4A NA
CHB C1B
CHB HHB
C1B NB
C1B C2B
NB C4B
NB HB
C4B C3B
C4B CHC
C3B C2B
C3B C6B
C2B CMB
CMB HMB1

```
  CMB    HMB2
  CMB    HMB3
  C6B      OB
  C6B     C7B
  C7B    H7B1
  C7B    H7B2
  C7B    H7B3
   NA     C1A
  C1A     CHA
  CHA     C4D
  CHA     CBD
  C4D      ND
  C4D     C3D
   ND      HD
   ND     C1D
  CBD     CGD
  CBD     HBD
  CBD     CAD
  CGD     O1D
  CGD     O2D
  O2D     CED
  CED    HED1
  CED    HED2
  CED    HED3
  CAD     OBD
  CAD     C3D
  C3D     C2D
  C2D     CMD
  C2D     C1D
  CMD    HMD1
  CMD    HMD2
  CMD    HMD3
  C1D     CHD
  CHD     HHD
  CHD     C4C
  C4C     C3CX
  C4C      NC
  C3CX    CAC
  C3CX    C2CX
  C3CX    H3CX
  CAC     CBC
  CAC    HAC1
  CAC    HAC2
  CBC    HBC1
  CBC    HBC2
  CBC    HBC3
  C2CX    C5C
  C2CX    C1C
  C2CX   H2CX
  C5C    H5C1
  C5C    H5C2
  C5C    H5C3
   NC     C1C
  C1C     CHC
  CHC     HHC

[ impropers ]
   C3      C1      C2       H2
   C2      C5      C3       C4
```

O2A	CBA	CGA	O1A
C2A	CHA	C1A	NA
C3A	CHB	C4A	NA
C1B	C4A	CHB	HHB
C1B	C4B	NB	HB
C4B	C2B	C3B	C6B
C3B	CHC	C4B	NB
C2B	CHB	C1B	NB
CMB	C3B	C2B	C1B
C4D	C1D	ND	HD
CBD	C4D	CHA	C1A
CBD	O2D	CGD	O1D
CBD	C3D	CAD	OBD
CAD	C4D	C3D	C2D
C3D	CHA	C4D	ND
C2D	CHD	C1D	ND
CMD	C1D	C2D	C3D
C1D	C4C	CHD	HHD
C3CX	CHD	C4C	NC
CAC	C2CX	C3CX	C4C
C2CX	CHC	C1C	NC